# Continuous-time quantum walks on multilayer dendrimer networks

Mircea Galiceanu[1,2,*] and Walter T. Strunz[2]
[1]*Departamento de Física, Universidade Federal do Amazonas, 69077-000 Manaus, Brazil*
[2]*Institut für Theoretische Physik, Technische Universität Dresden, 01062 Dresden, Germany*
(Received 18 May 2016; published 17 August 2016)

We consider continuous-time quantum walks (CTQWs) on multilayer dendrimer networks (MDs) and their application to quantum transport. A detailed study of properties of CTQWs is presented and transport efficiency is determined in terms of the exact and average return probabilities. The latter depends only on the eigenvalues of the connectivity matrix, which even for very large structures allows a complete analytical solution for this particular choice of network. In the case of MDs we observe an interplay between strong localization effects, due to the dendrimer topology, and good efficiency from the linear segments. We show that quantum transport is enhanced by interconnecting more layers of dendrimers.

DOI: 10.1103/PhysRevE.94.022307

## I. INTRODUCTION

In the past decade, complex network models have been used to explain a wide range of physical, chemical, biological, sociological, or economic systems (see [1–3] and references therein). In these works, statistical and dynamical features of networks were studied. A prime example is the Internet, which can be understood using the scale-free network model. It has as its main ingredient the existence of hubs, nodes with a high number of connections, and the degree distribution follows a power law [4,5]. A different kind of complex network model, the multilayer network or network of networks [6–12], has instigated continuously growing interest from the research community. These more complex networks are composed of a succession of interconnected layers, each of them containing the same number of nodes. Moreover, they have two types of links: those between nodes belonging to the same layer and links between nodes from different layers. Here, for simplicity and to facilitate an analytical solution, we consider layers with the same topology and each node is connected to one node from two neighboring layers (or one in the case of peripheral layers). As an example we choose as the underlying topology the dendrimer, which allows for analytical results [13,14].

From the classical point of view, the dynamics of random walks (RWs) on networks and its relation with the network's topology have been investigated for many decades [15]. The problem of transport efficiency amounts to determining the probability of the RW to return to its origin. As in the case of the classical random walk, the quantum mechanical transport is basically divided into two models: the discrete-time quantum walk and the continuous-time quantum walk. The concept of quantum walk was introduced by Aharonov *et al.* [16] and the discrete-time quantum walk, which requires an additional degree of freedom, the *coin*, was introduced by Meyer [17]. The continuous-time quantum walk is based on identifying the quantum mechanical Hamiltonian with the classical transfer matrix. It was introduced in the seminal paper of Farhi and Gutmann [18]. However, these two models can be related [19]. In this article we choose to follow the continuous model.

For any undirected network the transfer matrix of the continuous-time random walk (CTRW) is given by the connectivity matrix of the structure [20]. In order to correlate the results with the CTRW we choose the model of a continuous-time quantum walk (CTQW) to study the quantum transport on networks [21]. In this model the Hamiltonian is also determined from the connectivity matrix, as its classical counterpart. However, the quantum dynamics is more complex than the classical dynamics: Due to the propagation of *amplitudes* rather than probabilities, wave properties such as interference strongly influence the object (particle) dynamics. We know from the literature that for branched trees, such as dendrimers [22], the quantum transport efficiency is lower compared to translationally invariant graphs. In order to enhance the spreading of the quantum walks on graphs one should add more links to the given structure [23]. In this paper we focus on another way of increasing the efficiency of transport on a graph: Create a multilayer network, or more precisely, we couple the graph to copies of itself. Recently, such an approach was also considered in Ref. [24] for multiplex networks. In the case studied in this paper, however, we can provide a systematic theoretical study also for very large regular networks, facilitated by the fact that all the eigenvalues are known analytically. It is worth mentioning that our diagonalization method can be applied to any multilayer network, for which all the eigenvalues of its connectivity matrix of the underlying graph (the dendrimer in our case) are completely determined.

The problem of quantum transport in nontrivial topologies is of current interest due to its relevance for energy transfer in molecular (e.g., light harvesting) aggregates [25,26], due to quantum computing [27] and most remarkably due to an impressive increase in experimental techniques. These experiments allow for a better understanding of the theoretical models. They are based on ultracold atoms in optical lattices [28] or on microwave cavities [29], Rydberg atoms [30,31], atoms or ions trapped in optical lattices [32–34], or photons in waveguide arrays [35–38], on an optical circuit [39], or on an optical fiber network [40].

In presenting our results, we choose the following organization of the paper. In Sec. II we focus on a general description

*mircea@ufam.edu.br

 

of the classical and quantum quantities used throughout the paper. In Sec. III we show the construction principles of our multilayer dendrimer network. Section IV is devoted to the analytical determination of the eigenvalue spectrum of the connectivity matrix, necessary to compute all the physical (quantum and classical) quantities of our model. In Sec. V we focus on findings for quantum transport on networks and we compare our results to classical random walks. The paper ends with a summary.

## II. THEORETICAL FRAMEWORK

In this article we study the quantum dynamics of an excitation on multilayer networks in the CTQW model and compare these results with its corresponding classical model, the CTRW. In general, a network is defined as a set of $N$ nodes coupled to each other by bonds. A state $|k\rangle$ is associated with each node, corresponding to an excitation localized at node $k$. The CTRW and CTQW dynamics are determined by the connections between the nodes of the network, i.e., by the connectivity matrix $\mathbf{A}$. This $N \times N$ matrix is real and symmetric: Its nondiagonal elements $A_{jk}$ are equal to $-1$ if the $i$th and $j$th nodes are connected by a single bond and 0 otherwise, while the diagonal elements $A_{jj} = f_j$ equal the number of bonds $f_j$ connected to node $j$. Due to its construction, the connectivity matrix has only positive real eigenvalues and only one vanishing eigenvalue $\xi_{\min} = 0$.

For CTRWs in the simplest case, where the transition rates for all bonds are equal (and chosen to be 1), the transfer matrix is simply $\mathbf{T} = -\mathbf{A}$. The probability for a CTRW to go from node $k$ to node $j$ at time $t$ reads $p_{j,k}(t) = \langle j|\exp \mathbf{T}t|k\rangle$. For CTQWs we assume that all the states $|j\rangle$, which represent the nodes, are orthonormal and complete [18,21] and the dynamics is described by the quantum mechanical Hamiltonian, identified with $\mathbf{H} = \mathbf{A}$. In this case the quantum transition probabilities are given by $\pi_{j,k}(t) = |\langle j|\exp(-i\mathbf{H}t)|k\rangle|^2$. Knowing the eigenvalues $\xi_n$ and eigenstates $|\Phi_n\rangle$ (with $n = 1, \ldots, N$) of the connectivity matrix, we can write the transition probability for CTRWs as

$$p_{j,k}(t) = \sum_{n=1}^{N} \exp(-\xi_n t)\langle j||\Phi_n\rangle\langle\Phi_n||k\rangle \tag{1}$$

and for CTQWs as

$$\pi_{j,k}(t) = \left|\sum_{n=1}^{N} \exp(-i\xi_n t)\langle j||\Phi_n\rangle\langle\Phi_n||k\rangle\right|^2. \tag{2}$$

We focus on the average return probability as a measure of the transport efficiency. It is defined as the probability to remain or return to the initial node $k$, averaged over all nodes

$$\overline{p}(t) = \frac{1}{N}\sum_{k=1}^{N} p_{k,k}(t) \tag{3}$$

for CTRWs and

$$\overline{\pi}(t) = \frac{1}{N}\sum_{k=1}^{N} \pi_{k,k} \tag{4}$$

for CTQWs. A fast decay of $\overline{p}(t)$ or $\overline{\pi}(t)$ implies a quick propagation of a walker on the network and a slow decay implies a slow propagation. For CTRWs the average return probability simplifies considerably, such that it will depend only on the eigenvalues of the connectivity matrix

$$\overline{p}(t) = \frac{1}{N}\sum_{k=1}^{N} \exp(-\xi_k t), \tag{5}$$

and for CTQWs $\overline{\pi}(t)$ additionally depends on the eigenstates. However, by making use of the Cauchy-Schwarz inequality we get a lower bound, which is independent of the eigenstates:

$$\begin{aligned}\overline{\pi}(t) &= \frac{1}{N}\sum_{k=1}^{N} \pi_{k,k} \geqslant \left|\frac{1}{N}\sum_{k=1}^{N} \alpha_{k,k}(t)\right|^2 \\ &= |\overline{\alpha}(t)|^2 = \left|\frac{1}{N}\sum_{k} \exp(-i\xi_k t)\right|^2. \end{aligned} \tag{6}$$

In Eq. (6) we defined the transition amplitude between two nodes as $\alpha_{k,k} = \langle k|\exp(-i\mathbf{H}t)|k\rangle$. From Eq. (5) one gets in the long-time limit the equipartition value $1/N$. In the quantum case, $\overline{\pi}(t)$ and $|\overline{\alpha}(t)|^2$ do not decay to a fixed value, but they oscillate around the long-time average [21]

$$\chi \equiv \lim_{t\to\infty}\frac{1}{t}\int_0^t dt'|\overline{\alpha}(t')|^2 \leqslant \lim_{t\to\infty}\frac{1}{t}\int_0^t dt'\overline{\pi}(t') \equiv \overline{\chi}. \tag{7}$$

Knowing the spectral density $\rho(\xi)$, one can write the long-time average transition probability as [41,42]

$$\chi = \sum_{\xi}\rho^2(\xi) \geqslant \rho^2(\xi^*) + \frac{1}{N}[1 - \rho(\xi^*)] \equiv \chi^*, \tag{8}$$

where $\xi^*$ is the most degenerate eigenvalue. As stated in Ref. [41] $\chi^*$ provides a good approximation of $\chi$ in two extreme situations. The first one corresponds to the case of $\xi^*$ being a single highly degenerated eigenvalue in comparison with the other eigenvalues, for instance, for a star with $N-1$ arms. In this case, there will be only three eigenvalues, namely, 0, 1, and $N$, with degeneracies 1, $N-2$, and 1, respectively; thus it is straightforward to show that $\chi = \chi^* = [2 + (N-2)^2]/N^2$. In the limit of very large structures, we obtain $\chi_\infty = 1$, suggesting an inefficient transport. The second situation occurs when all the eigenvalues are nondegenerate, which occurs, for example, for a linear chain. In this case all the eigenvalues have degeneracy $\rho(\xi) = 1/N$, which yields $\chi = \chi^* = 1/N$. For extremely long chains we get an efficient transport $\chi_\infty = 0$.

## III. MULTILAYER DENDRIMER NETWORKS

We consider our multilayer structure as a sequence of, say, $L$ layers, each of them being identical copies of the original layer. Here we choose as the original layer the dendrimers and we denote by $G$ their generation number. All the nodes from a layer are connected to a single node from the neighboring layers (two layers for inner layers and one neighbor for peripheral layers). We can divide the construction of this multilayer dendrimer network (MD) into two parts. The first one corresponds to the construction of the basic

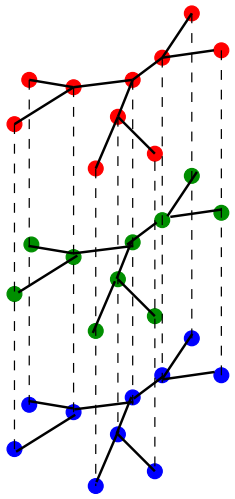

FIG. 1. Multilayer dendrimer with generation number $G = 2$ and $L = 3$ layers.

structure (in our case the dendrimer), while the second part represents the reproduction ($L$ times) of the above structure and the connection to nodes from next-nearest-neighbor layers according to our prescription.

The construction of a dendrimer follows the steps well established in the literature [14,43]. One starts from a central node (generation 0) and adds $f$ (in our case $f = 3$) nodes, all connected to the central node. These nodes correspond to the first generation. Then, from each node of the first generation sprout another $f - 1$ bonds, inserting $f - 1$ new nodes into the structure, all of them forming the second generation. This process is iterated until we reach the desired generation $G$. Each internal node of the dendrimer has $f = 3$ neighbors and the peripheral nodes, i.e., nodes from generation $G$, have $f - 2 = 1$ neighbors from the previous generation. The total number of nodes of a dendrimer of generation $G$ and functionality $f$ equals [14] $N_D = 3[(f-1)^G - 1]/(f-2) + 1$, which for a dendrimer with functionality $f = 3$ becomes

$$N_D = 3(2^G - 1) + 1. \tag{9}$$

Next, in the second part of the construction, we copy $L$ times the above structure (the dendrimer of generation $G$) and connect all nodes of an internal layer $j$ with the nodes belonging to its neighboring layers $j - 1$ and $j + 1$. Each node of the peripheral layer is connected to a single node from the neighboring layer. Thus, the total number of nodes of a MD equals $N_{\mathrm{MD}} = LN_D$. In Fig. 1 we sketch the multilayer dendrimer of generation number $G = 2$ and having three identical layers $L = 3$. For a better visualization, each layer's nodes are depicted with the same color, the connections between nodes belonging to the same layer are displayed with solid lines, and the links between nodes of different layers are shown with dashed lines.

## IV. EIGENVALUE SPECTRUM

One can clearly see from Eqs. (5) and (6) that we need to determine the whole eigenvalue spectrum of the connectivity matrix $\mathbf{A}$ for the MD. The connectivity matrix is a real and symmetric sparse matrix and for this particular topology we are able to analytically compute all the eigenvalues. The matrix $\mathbf{A}$ has the size $N_{\mathrm{MD}} \times N_{\mathrm{MD}} \equiv (LN_D) \times (LN_D)$ and it is composed of blocks of square submatrices $\mathbf{A_{ij}}$ of $N_D \times N_D$ size, where $L$ represents the number of layers from the MD and $N_D$ is the number of nodes in each layer. The matrix $\mathbf{A}$ is a block matrix and it is defined as follows: The off-diagonal blocks equal $\mathbf{A_{ij}} = -\mathbb{1}$ if layers $i$ and $j$ are connected and $\mathbf{A_{ij}} = \mathbf{0}$ otherwise. Here $\mathbb{1}$ is the identity matrix and $\mathbf{0}$ is the matrix having all its elements equal to 0. The diagonal block matrices are given by $\mathbf{A_{ii}} = \mathbf{A_L} + 2 \times \mathbb{1}$ if $i$ is an inner layer $1 < i < L$ and $\mathbf{A_{ii}} = \mathbf{A_L} + \mathbb{1}$ if $i$ is a peripheral layer, namely, $i = 1$ or $i = L$. Here $\mathbf{A_L}$ is the connectivity matrix of a single dendrimer.

We define the eigenvalue spectrum of the MD as $\Xi_{\mathrm{MD}} = (\Xi_0, \Xi_1, \ldots, \Xi_j, \ldots, \Xi_{L-1})$, where $\Xi_0$ contains the first $N_D$ eigenvalues, $\Xi_1$ the next $N_D$ eigenvalues, and so on up to the last eigenvalue. The eigenvalues of each set of eigenvalues $\Xi_j$ can be written as [6]

$$\Xi_j = 2 - 2\cos\left(\frac{j\pi}{c}\right) + \xi_i, \tag{10}$$

where $j = 0, 1, \ldots, L-1$ denotes the number of the layer, $\xi_i$ are the eigenvalues of the connectivity matrix $\mathbf{A_L}$ of a single layer, and here we have $i = 1, \ldots, N$. The eigenvalues $\xi_i$ can be found by implementing a normal mode analysis and by making use of the symmetries of the structure [14,43,44]. Following this procedure, one is able to find analytically all the eigenvalues and end up with a simple physical explanation of the normal modes. For every network there are two groups of eigenmodes: the symmetric modes, when all the nodes are oscillating, and nonsymmetric modes, when some nodes (including the central core) are immobile. In our quantum mechanical excitation transport picture, any vibration of the nodes of the dendrimers can be understood as a linear combination of all $N_{\mathrm{MD}}$ normal nodes.

In the following we will not present the detailed evaluation of the eigenvalues, since our main focus is their influence on properties of quantum walks. Instead, we only summarize how the whole spectrum of a trifunctional dendrimer, i.e., dendrimer of functionality $f = 3$, is obtained. For a dendrimer of generation number $G$ there are $G$ symmetric modes with their nondegenerate eigenvalues given by [14,43]

$$\xi_k^{(s)} = 3 - 2\sqrt{2}\cos\left(\frac{\pi k}{G+1}\right) \quad \text{for } k = 1, \ldots, G. \tag{11}$$

In addition, we have the totally symmetric eigenvalue $\xi_{G+1}^{(s)} = 0$, which corresponds to an overall translational motion. Then all the nodes vibrate in the same direction and with the same magnitude.

The second group of eigenvalues is formed by modes that have an immobile core. This class contains nonsymmetric eigenmodes with degenerate eigenvalues. In the special case when only one central node ($G = 0$) is immobile, the eigenvalues are determined by solving a system of two equations

$$\xi_k^{(n)} = 3 - 2\sqrt{2}\cos\psi_k \tag{12}$$

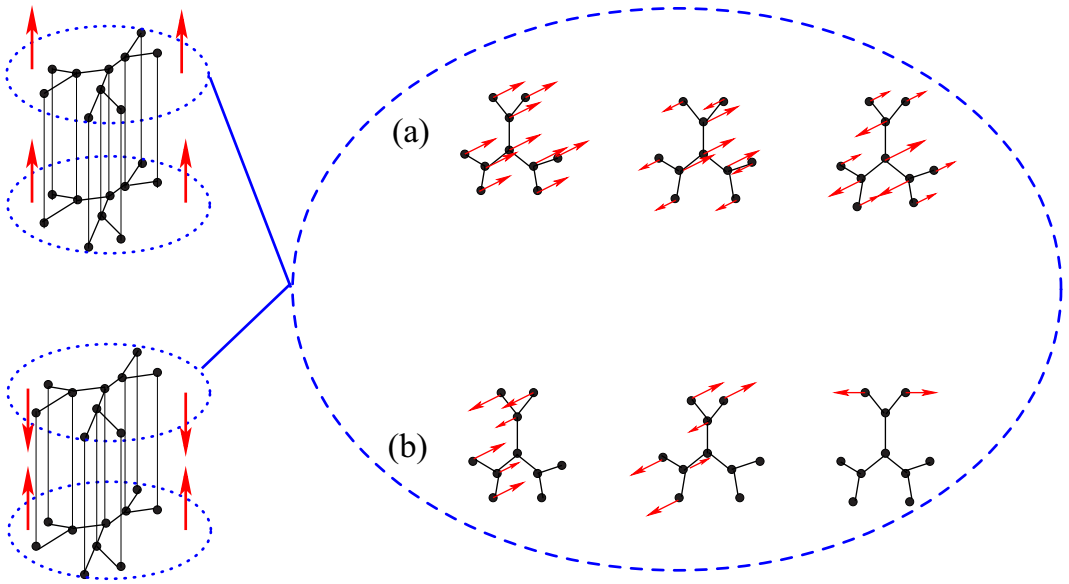


FIG. 2. Normal modes for a multilayer dendrimer network of $G = 2$ and $L = 2$.

and

$$\sin(G+1)\psi_k = \sqrt{2}\sin G\psi_k. \tag{13}$$

For $G < 3$ Eqs. (12) and (13) provide $G$ distinct solutions. For $G \geqslant 3$ these equations give only $G-1$ solutions. Then there is one hyperbolic eigenvalue, which has the form

$$\Xi^{(n)} = 3 - 2\sqrt{2}\cosh\psi, \tag{14}$$

where $\psi$ fulfills the equation

$$\sinh(G+1)\psi = \sqrt{2}\sinh G\psi. \tag{15}$$

All these $G$ eigenvalues for this particular case are doubly degenerate.

In more general cases there are more nodes that remain immobile, apart from the central node, and the eigenvalues are still given by Eq. (12) with $\psi_k$ now obeying

$$\sin(G+1-m)\psi_k = \sqrt{2}\sin(G-m)\psi_k, \tag{16}$$

where we have denoted by $m$ (with $0 < m < G-1$) the last generation number in which all the nodes are immobile. Equation (16) has $G-m$ distinct solutions if $G-m+1 > \sqrt{2}(G-m)$. Otherwise, there are $G-m-1$ distinct eigenvalues of the form (16) and an additional eigenvalue of hyperbolic form given by Eq. (14) with $\psi$ obtained from

$$\sinh(G-m+1)\psi = \sqrt{2}\sinh(G-m)\psi. \tag{17}$$

Thus, for every $m$ there are $G-m$ distinct eigenvalues and each of them is $(3\times 2^{m-1})$-fold degenerate. Finally, there is the special case of $m = G-1$ that gives rise to a $(3\times 2^{G-2})$-fold degenerate eigenvalue $\xi = 1$, corresponding to all pairs of peripheral nodes from the same branch, oscillating in opposite directions.

For a deeper understanding of the results we choose a small multilayer dendrimer network and we display in Fig. 2 its normal modes. Our chosen network has generation number $G = 2$ and two layers. For this particular example there are two types of eigenmodes, shown on the left side of the figure, which can be analytically obtained from Eq. (10) by deploying $j = 0$ and 1. The first value corresponds to the situation when the nodes from the two layers oscillate in the same fashion and with the same magnitude; while the second value $j = 1$ corresponds to the case where the nodes from one layer oscillate in the same manner but in opposite direction compared to nodes belonging to the other layer. Thus, one can envisage this by two layers moving in the same direction and by the layers moving in opposite directions, respectively. The eigenvalues of the first situation are the same as for a single dendrimer of the same generation number, as can be easily seen from Eq. (10) by substituting $j = 0$. The eigenvalues corresponding to the second class of eigenmodes are obtained by replacing $j = 1$ in Eq. (10), thus they are shifted by 2 from the single dendrimer's eigenvalues. In the right panel of Fig. 2 we display all the eigenmodes of a single dendrimer layer. In Fig. 2(a) we show the $G+1$ symmetric eigenmodes, i.e., all the nodes are oscillating, namely, $\xi^{(s)} = 0$ (which represents the overall translation), 2, and 5, in which monomers from the same generation move together. In Fig. 2(b) there are the nonsymmetric eigenmodes, from left to right: $\xi^{(n)} = 2-\sqrt{3}$ and $\xi^{(n)} = 2+\sqrt{3}$, both with degeneracy 2, in which the nodes of the two branches move in opposite directions, and $\xi^{(n)} = 1$ with degeneracy 3, which represents the motion of two connected peripheral nodes, respectively. Thus, summing up all the eigenvalues and their degeneracies, we have ten eigenmodes for the first class (layers oscillate in the same direction) and another ten eigenmodes for the second class (layers oscillating in opposite directions).

## V. RESULTS

### A. Space-time structures

First, we focus on three distinct small multilayer dendrimer networks and study the quantum mechanical transition probabilities in the framework of the CTQW model. In Fig. 3 we

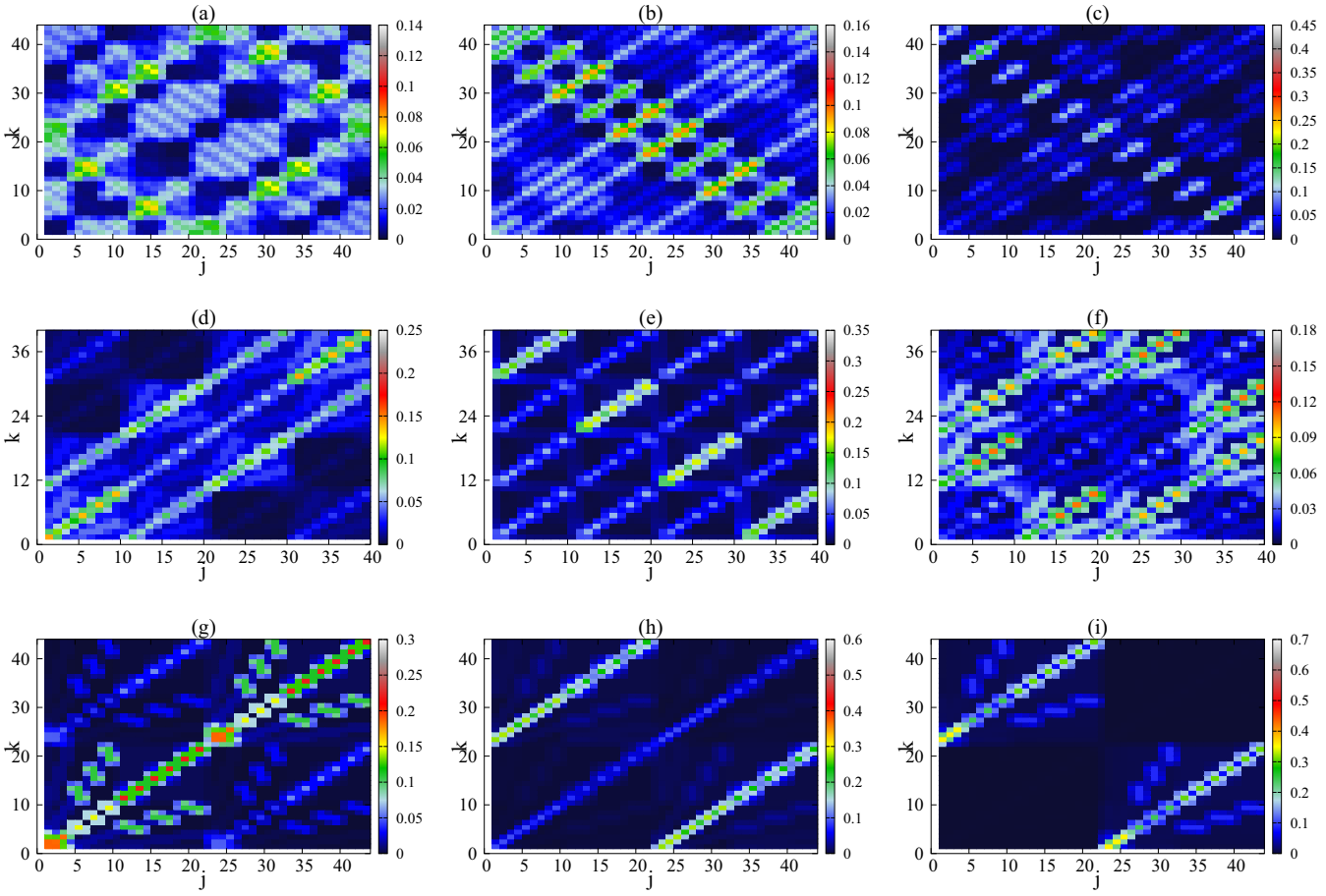


FIG. 3. Contour plots of the probability for a CTQW to start at node $k$ and to be encountered at node $j$ after times $t = 10$ (left column), $t = 20$ (middle column), and $t = 30$ (right column) for the following sets of MD parameters: (a)–(c) $(G,L,N_D) = (1,11,4)$, (d)–(f) (2,4,10), and (g)–(i) (3,2,22).

show the probability $\Pi_{j,k}$ of a CTQW to start at node $k$ and to be at node $j$ after a certain time, given by Eq. (2), for small MDs. For comparison, we choose three particular cases of multilayer dendrimers with almost the same total number of nodes. The first case corresponds to a long and thin MD with $L = 11$ layers and a generation number $G = 1$ of the dendrimer [Figs. 3(a)–3(c)]. The second case is a compact MD with its dendrimer extension equal to the number of layers, with $G = 2$ and $L = 4$ [Figs. 3(d)–3(f)], and the last one is a large MD made of dendrimers of higher generation $G = 3$, but only $L = 2$ layers [Figs. 3(g)–3(i)]. The probabilities for three different times are shown in Fig. 3, namely, $t = 10$, 20, and 30 from left to right, respectively. For a long and thin MD (first case) and $t = 20$ one can easily notice larger probabilities on the antidiagonal, i.e., walkers that started at $t = 0$ from the first layer are now more likely localized on the last two layers and so on. Increasing the time to $t = 30$, we observe a visible mixture of regions with higher probabilities (green in the figure) and low probabilities (blue). The highest probability, equal to 0.41, was encountered for a CTQW that started at node 5 (center of the second layer), which at time $t = 30$ is located at node 37 (center of the tenth layer) $\Pi_{37,5}(30)$. For the most compact MD, with $G = 2$ and $L = 4$, the localization effects on layers are immediately apparent and the transport is more efficient through the bonds between layers. For $t = 20$ (middle snapshot) one can see that all walkers end up having higher probabilities at a central node belonging to any of the four layers. However, this situation becomes smoother at time $t = 30$, when we encounter a very mixed pattern with fewer very low or very high probabilities. The highest probability equals 0.17 and is obtained in 24 situations corresponding to a walker that starts at one node from a layer's periphery and ends up at another peripheral node of the next neighboring layer, for example, $\Pi_{5,16}$, $\Pi_{6,15}$, $\Pi_{25,36}$, and $\Pi_{26,35}$. The second highest probability is 0.16, which is encountered also 24 times, corresponding to a walk between any peripheral node of a layer and another peripheral node from the next-nearest-neighbor layer, for instance, $\Pi_{5,26}$ and $\Pi_{6,25}$. The last case, which corresponds to a MD with $G = 3$ and $L = 2$, is displayed in the last three snapshots of Fig. 3. Here the localization effects are dominate for all the times, because there are more nodes belonging to a dendrimer than linear segments. For instance, in the snapshot of $t = 30$ one can clearly notice that all the walks have 0.66 as their highest probability and physically this means that a walk that started at a certain node reaches its corresponding node from the other layer.

In Fig. 4 we have the same three types of small MDs as in Fig. 3. Here we monitor the time evolution of $\Pi_{j,k}(t)$ [Eq. (2)] for some particular starting points and we display the results

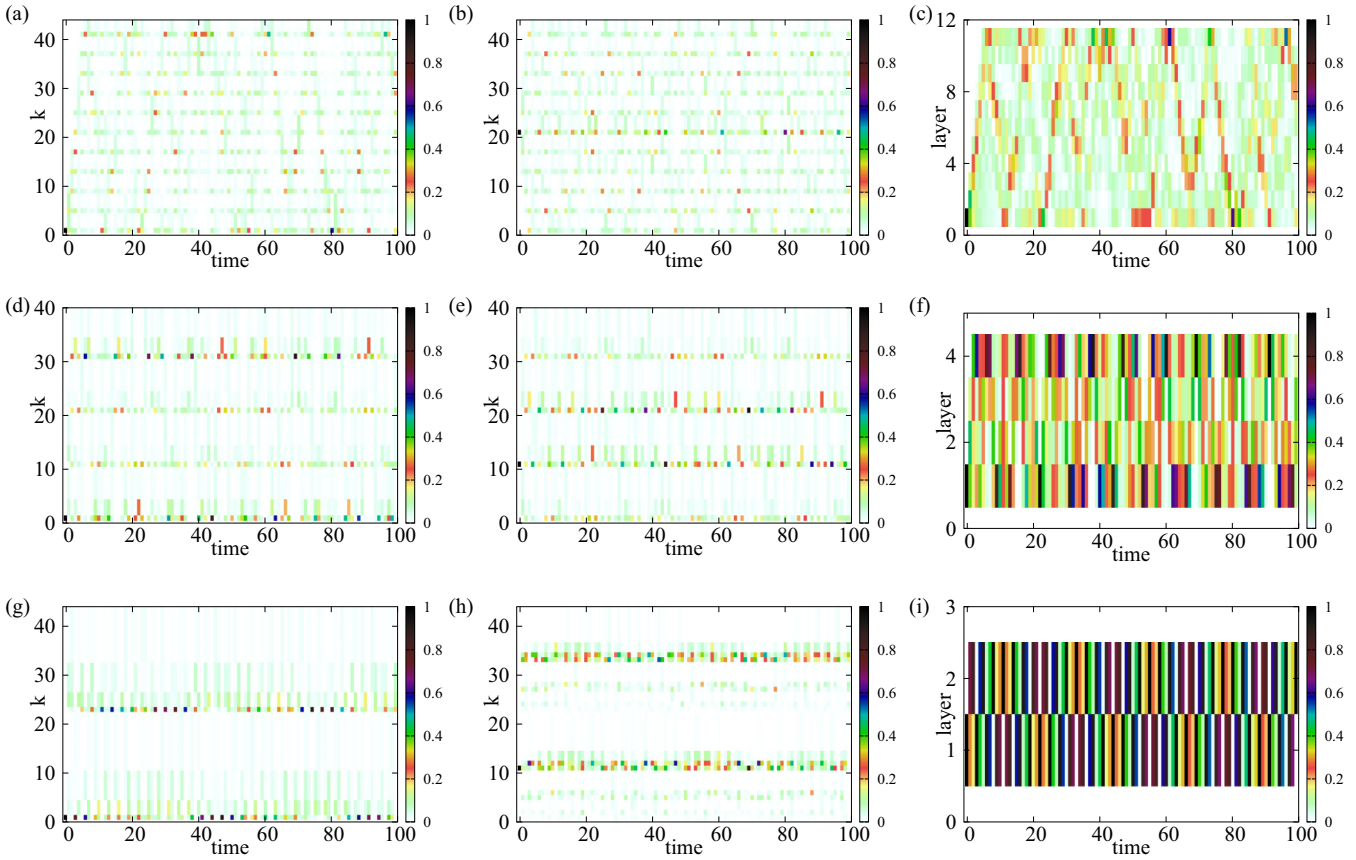


FIG. 4. Contour plot of the probability $\Pi_{j,k}$ for a CTQW on some small MD, namely, (a)–(c) $(G,L,N_D) = (1,11,4)$, (d)–(f) (2,4,10), and (g)–(i) (3,2,22), as a function of time $t$. The starting node of the walker corresponds to the central node $k = 1$ of the peripheral layer (left and right columns) and to the central node $k = 21$ (middle column, top row), central node $k = 11$ (middle column, middle row), and peripheral node $k = 11$ (middle column, bottom row) of the middle layer.

only for integer values of time. As for single dendrimers, it is worth mentioning that also for MDs the transition probabilities from the central node to nodes belonging to the same generation are equal due to rotational symmetry. Thus, there is no need to study CTQWs for all possible starting nodes of the excitation. The first column of Fig. 4 corresponds to walks for which the starting point is the central node of the first layer $k = 1$. For all three classes the walk is mainly localized at the central nodes of the layers, with higher probabilities for MDs with fewer layers. For all three small structures the walker will return to the origin at different times and with different magnitudes. It is important to stress that, due to the complexity of the structures, an analytical expression for the revival time, computed for ring chains [21], is not possible. The revival time $\overline{\tau}$ is obtained by solving the equation $\alpha_{j,k}(\overline{\tau}) = \alpha_{j,k}(0)$, where $\alpha_{j,k}$ is the transition amplitude between two nodes [see Eq. (6)]. However, only for small rings we encounter a full revival of the initial condition; in general, we obtain partial revivals. For our structures we understand by (incomplete) revival time $\tau$ the numerically obtained time for which the probability $\Pi_{j,k}$ is higher than 0.5. For our first structure with $G = 1$ and $L = 11$, the revival time $\tau$ equals 80 and the initial localization (at node 1) is only partially retrieved, $\Pi_{1,1}(80) \approx 0.59$. For the second network with $G = 2$ and $L = 4$ the revival time is shorter $\tau = 44$, but the return probability is higher, $\Pi_{1,1}(44) \approx 0.86$, while for the third structure with $G = 3$ and $L = 2$ we obtain the partial revival $\Pi_{1,1}(\tau = 47) \approx 0.91$. It is important to mention that for the last structure we encounter high values for the probability $\Pi_{j,k}$ also at earlier times, such as $t = 3,6,41$, giving weight to our statement that MDs with a low number of layers lead to very strongly localized walks. We find more such values by considering also noninteger values of time, as it will be shown in Fig. 5. In the second column of Fig. 4 we show results for the probability of a walker being at node $k$ starting from node 21 [Figs. 4(a)–4(c)] and node 11 [Figs. 4(d)–4(i)]. Notice that 21 in the top row corresponds to the central node of the sixth layer, i.e., it is the node at the middle of the structure of the first MD. Node 11 in Figs. 4(d)–4(f) corresponds to the central node of the second layer, for the second MD considered. Finally, node 11 for Figs. 4(g)–4(i) is situated at the periphery of the first layer of the third MD.

From all these frames one can see that the walks have higher probabilities to be localized at the initial starting point and at their corresponding nodes from other layers. This fact strengthens our observation that the walker travels faster along the linear segments than along the dendrimer's segments of the layers. Thus, an MD will experience two opposing effects related to their mixed topologies, namely, a fast dynamics arising from the linear segments and a strong localization

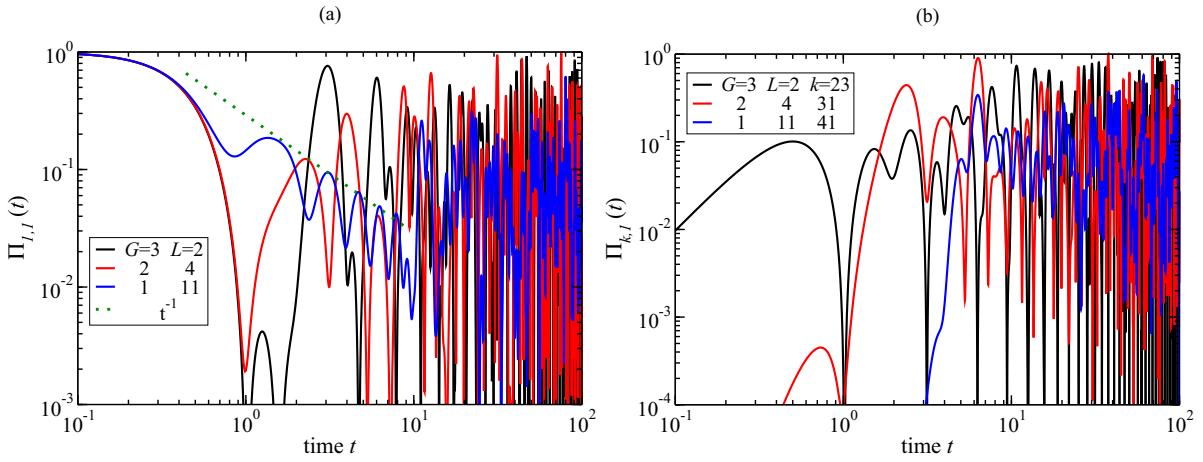


FIG. 5. Probability $\Pi_{j,k}(t)$ for CTQW on three small multilayer dendrimer networks having as the starting node the origin $k = 1$ and as the ending node (a) the origin and (b) the central node of the last layer.

due to the dendrimer parts of the network. In the rightmost column of Fig. 4 we monitor the probability of the walk being situated on a particular layer starting from the central node of the first layer, node 1. For the first case (MD with $L = 11$ layers), we notice a more disperse situation, which is similar to the linear chain [21] due to the fact that the linear segments are predominant here too. As in Figs. 4(a) and 4(b) of this particular MD the incomplete revival time also occurs at $\tau = 80$, with $\Pi_{1,\text{layer1}} \approx 0.61$. For the second MD considered here, we observe that the walker returns more frequently to the first layer and its return probability gets higher than in the previous case: $\Pi_{1,\text{layer1}}(\tau = 9) \approx 0.84$, $\Pi_{1,\text{layer1}}(22) \approx 0.96$, or $\Pi_{1,\text{layer1}}(31) \approx 0.88$, to name a few. One can also see that even though the probability for the walk to be on one of the two peripheral layers gets very high for some values of time, the probability to be on either of the inner layers (2 or 3) is quite low. Its maximum is encountered at time $t = 2$ and equals 0.45. In the last case, the MD with $G = 3$ and $L = 2$, we observe an alternation of high and low probabilities, since the MD contains only two layers.

For a more detailed picture of the walker's time evolution we plot in Fig. 5 the probability to return $\Pi_{1,1}(t)$ [Fig. 5(a)] and the probability to reach the center node of the last layer $\Pi_{j,1}(t)$ [Fig. 5(b)]. Here we choose the same three small multilayer dendrimer networks used in the previous two figures, but in contrast we display also noninteger values of time. As observed in Fig. 4, the walker returns to the origin with higher probability for MD with fewer layers. For the multilayer dendrimer network with $G = 3$ and $L = 2$ one can easily notice many peaks with probabilities higher than 0.5, with the most pronounced peaks being at $\Pi_{1,1}(46.95) \approx 0.92$, $\Pi_{1,1}(43.85) \approx 0.86$, and $\Pi_{1,1}(90.79) \approx 0.84$. Remarkably, the second network, with $G = 2$ and $L = 4$, shows higher values for the probability to return, which were also were encountered at earlier times. This is due to the mixture of strong localization effects, which is a feature of the dendrimer's topology, and higher spreading from and to the origin, which is a feature of linear chain's topology. The highest values are $\Pi_{1,1}(75.41) \approx 0.98$, $\Pi_{1,1}(31.38) \approx 0.93$, and $\Pi_{1,1}(44.04) \approx 0.87$. For the MD with a higher number of layers with $G = 1$ and $L = 11$, we encounter fewer points with probability higher than 0.5 and the maximum is $\Pi_{1,1}(80.08) \approx 0.61$. The walker initially evolves by following the linear chain's behavior, namely, a power-law decay with exponent $-1$, which is displayed by the dotted line in the figure and is more evident for the multilayer with 11 layers. From Fig. 5(b) we also notice that the probability to reach the center of the last layer is higher for the MD with fewer layers, due to dendrimer's predominance. The network with $G = 3$ and $L = 2$ has the highest number of points with probability higher than 0.5, having the maximum $\Pi_{23,1}(74.04) \approx 0.90$. However, the structure with $G = 2$ and $L = 4$ shows stronger localization properties, having higher values for the probability with its maximum $\Pi_{31,1}(37.71) \approx 0.99$. The small MD with $G = 1$ and $L = 11$ has fewer points with high probability with their magnitude being lower: Its maximum is $\Pi_{41,1}(61.21) \approx 0.57$. The multilayer dendrimer networks with fewer layers reach the region of high probabilities faster.

### B. Average return probabilities

In Fig. 6 we show the average probability for the excitation to return to its initial starting point. Both the classical CTRW $\overline{p}(t)$ [Eq. (5)] and the quantum mechanical CTQW $|\overline{\alpha}(t)|^2$ [Eq. (6)] are considered. Here, to render the comparison easier we choose networks with almost the same number of nodes, but with vastly different topologies. We display results for two limiting cases: a very long linear chain, with $G = 0$ and $L = 98\,302$, and a very large dendrimer, with $G = 15$ and $L = 1$, both structures having a total of $N = 98\,302$ nodes. The third structure is an MD composed of interconnected dendrimers of generation $G = 11$ and $L = 16$ layers, corresponding to $N = 98\,272$ nodes. The asymptotic behavior of the classical average probability $\overline{p}(t)$ at very long times, namely, a $1/N$ dependence, is reached for all three structures, but at different times. Remarkably, the multilayer dendrimer network gets to the equipartition value faster than the other two structures. This can be explained by the fact that MD contains a high number of nodes with functionality higher than the nodes of one-layer dendrimers. In the intermediate time domain the classical average probability $\overline{p}(t)$ shows a power law with slope $-0.5008$ for the line, similar to the expected theoretical

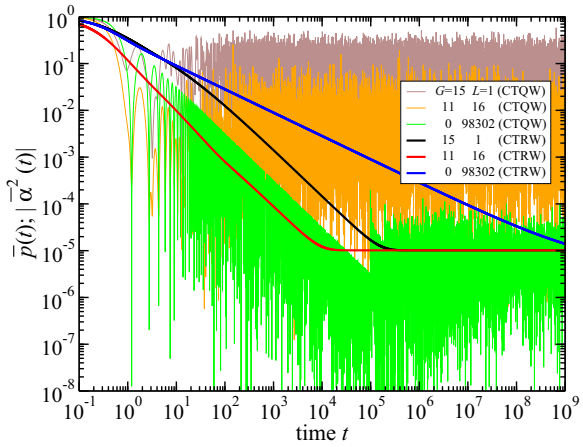


FIG. 6. Comparison between quantum (CTQW) and classical (CTRW) average return probabilities for multilayer dendrimers with almost the same number of nodes, but with totally different geometry: a lone large dendrimer ($G = 15$), a linear chain with $N = L = 98\,302$ nodes, and a mixed situation ($L = 16$ layers of dendrimers with generation number $G = 11$).

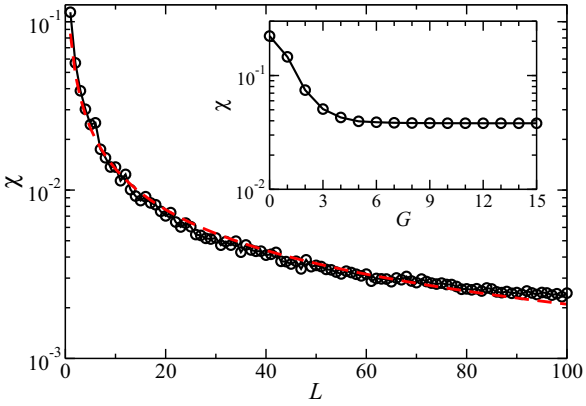


FIG. 7. Long-time average $\chi$ for multilayer dendrimers with fixed generation number $G = 6$ and a variable number of layer $L$. The inset shows $\chi$ for a fixed number of layers $L = 3$ and different generation number.

value $1/2$, and an exponential decay $\exp(-0.0563t)$, followed by another power law of slope $-0.9744$ for the dendrimer. For the MD considered we obtained a power-law behavior with slope $-1.0417$, while the exponential behavior gets very short. Now we turn our attention to the quantum mechanical average probability $|\overline{\alpha}(t)|^2$. Immediately apparent is the behavior for the linear chain, which follows the $t^{-1}$ decay at intermediate times and fluctuates around the long-time average at long times, as obtained also in Ref. [21]. For a single dendrimer the situation changes: The walks stay in a region close to the initial node. The transport to other distant nodes is highly unlikely, meaning that at long times the probabilities $|\overline{\alpha}(t)|^2$ and $|\overline{\pi}(t)|$ for any excitation to reach other nodes of the dendrimer stay very low. For our MD considered, with $G = 11$ and $L = 16$, we obtain a mixed situation because we have a combination of two topologies: linear and dendrimer. The oscillating behavior is also observed at short times, as for dendrimers. However, the dynamics is no longer as localized as in the single dendrimer case. Here the addition of connections between various dendrimer layers enhances a long-range dynamics, the excitation has higher probability to reach other branches of the dendrimer.

### C. Quantum transport

Finally, we monitor quantum transport on MDs by focusing on the long-time average $\chi$ and its approximation $\chi^*$, as given by Eq. (8). We regard the quantum transport as being efficient if $\chi$ is small, with its maximum efficiency at $\chi = 0$, and inefficient if $\chi$ approaches one. In Fig. 7 we plot in logarithmic scale $\chi$ for MDs with the same generation number $G = 6$, but a variable number of layers $L$ ranging from 1 to 100. In this way we are able to monitor the transition from a dendrimer behavior to a predominant linear chain behavior. For each set of parameters $(G, L)$ we compute the eigenvalue spectrum of the connectivity matrix $\mathbf{A}$, using the results from Sec. IV. Substituting into Eq. (8), we determine the quantum mechanical lower bound $\chi$. For $L = 1$, i.e., a single dendrimer, we obtain the value 0.11, which is close to the theoretical value [41] of $\chi_D^\infty = 1/9$. By a continuous increase of the number of layers we switch to a predominantly linear topology and the value of $\chi$ gets lower. In this case $G = 6$, in the limit of a very large number of layers we observe a tendency to a constant value for $\chi$, equal to 0.0023. In Fig. 7 we present by a dashed red line the best fit, namely, a power law $\chi \propto L^{-0.8}$. Regarding the quantum transport efficiency, we clearly observe an increase in efficiency by almost two orders of magnitude if the dendrimers are connected in a multilayer network fashion. In the inset of Fig. 7 we display $\chi$ for MDs with the same number of layers $L = 3$, but formed by dendrimers with different generation numbers. In this case, for dendrimers with a large generation number, we encounter the constant value of 0.038, which is close to the value of the above-proposed fitting parameter $\chi_D/L^{0.8} \approx 0.046$.

In Fig. 8 we plot the results for the transport efficiency measure $\chi$ and its approximation $\chi^*$ [Eq. (8)] for MDs with generation number $G$ and number of layers $L$ as a function of both parameters $(G, L)$. The left panel corresponds to the exact $\chi$ and the right panel is the approximation $\chi^*$. For a better visualization we display these results in logarithmic scale as a three-dimensional plot. The quantum transport on these networks is better enhanced by adding more layers to a given dendrimer than by increasing the generation number of the underlying dendrimer. The lowest value of $\chi$, which corresponds to $(G, L, N_{\mathrm{MD}}) = (15, 31, 3\,047\,362)$, equals 0.0046. This value represents an increase in the transport efficiency on MDs relative to a single dendrimer, with $\chi_D^\infty = 1/9 \approx 0.111$. Still, it is higher if compared with a line: $\chi_{\mathrm{line}}^N = 1/N$. However, by keeping constant the dendrimer's generation number and increasing the number of interconnected layers, $\chi$ gets lower, meaning that the quantum transport efficiency is higher. As for the approximate $\chi^*$, we only observe the same trend as $\chi$, but this approximation does not hold for these structures. This is due to the fact that the eigenvalue spectrum is not as discrete as in the case of single treelike structures [41]. In particular, for a single dendrimer of generation $G$ the most degenerate eigenvalue equals 1 and its degeneracy is $3 \times 2^{G-2}$.

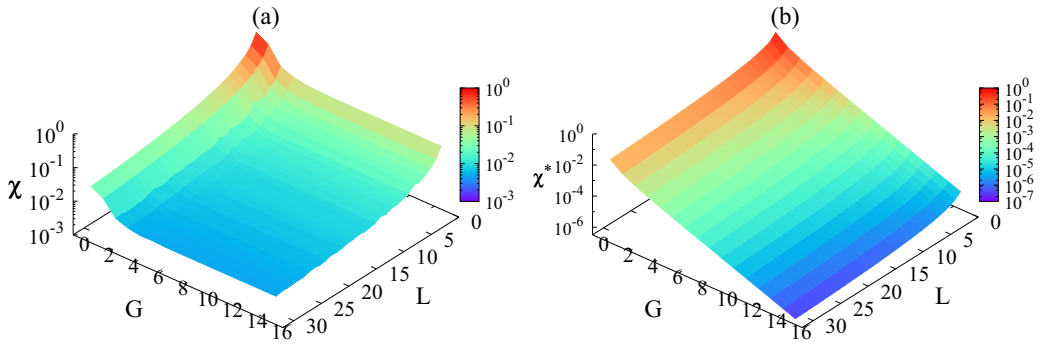


FIG. 8. Long-time average $\chi$ and its approximation $\chi^*$ for multilayer dendrimers.

Substituting in Eq. (8) one gets $\chi^* = (N^2 + 16N - 4)/16N^2$, which for very large dendrimers becomes $1/16$.

## VI. CONCLUSION

In this article we have focused on continuous-time quantum walks on multilayer dendrimer networks, which are constructed by adding identical layers on top of each other and connecting them with their nearest neighbors. We have monitored how the quantum mechanical transport is influenced by increasing the number of layers. In the continuous-time quantum walk model all physical quantities can be related to the eigenvalues of the connectivity matrix. Deploying the normal mode analysis, the eigenvalues for multilayer dendrimer networks were computed analytically in a straightforward manner. In this way we managed to increase the size of the networks, which allowed us to monitor the transition between predominant dendrimerlike to predominant linear topology. For a single dendrimer, the quantum walks remain localized at the starting point, while for a line the propagation of the walk is fast. We have shown that the slow quantum mechanical transport observed for dendrimers can be overcome by increasing the number of layers. We expect our results to be of interest in several areas, such as quantum and classical transfer of excitons, quantum transport on graphs, or quantum computing, to name only a few.

## ACKNOWLEDGMENTS

We thank Kimmo Luoma and Marcus Beims for fruitful discussions and DAAD/CAPES for support through PROBRAL. M.G. acknowledges support from the Brazilian research agency CNPq.

[1] M. Newman, *Networks: An Introduction* (Oxford University Press, New York, 2010).
[2] E. Estrada, *The Structure of Complex Networks* (Oxford University Press, New York, 2011).
[3] M. Barthélemy, Phys. Rep. **499**, 1 (2011).
[4] A. L. Barabási and R. Albert, Science **286**, 509 (1999).
[5] M. Galiceanu, Phys. Rev. E **86**, 041803 (2012).
[6] A. Volta, M. Galiceanu, A. Jurjiu, T. Gallo, and L. Gualandri, Mod. Phys. Lett. B **26**, 1250055 (2012).
[7] M. Kurant and P. Thiran, Phys. Rev. Lett. **96**, 138701 (2006).
[8] S. V. Buldyrev, R. Parshani, G. Paul, H. E. Stanley, and S. Havlin, Nature (London) **464**, 1025 (2010).
[9] S. Gómez, A. Díaz-Guilera, J. Gómez-Gardeñes, C. J. Pérez-Vicente, Y. Moreno, and A. Arenas, Phys. Rev. Lett. **110**, 028701 (2013).
[10] R. G. Morris and M. Barthelemy, Phys. Rev. Lett. **109**, 128703 (2012).
[11] G. D'Agostino and A. Scala, *Networks of Networks: The Last Frontier of Complexity* (Springer, Heidelberg, 2014).
[12] S. Boccaletti, G. Bianconi, R. Criado, C. I. del Genio, J. Gómez-Gardeñes, M. Romance, I. Sendiña-Nadal, Z. Wang, and M. Zanin, Phys. Rep. **544**, 1 (2014).
[13] A. A. Gurtovenko, Y. Y. Gotlib, and A. Blumen, Macromolecules **35**, 7481 (2002).
[14] C. Cai and Z. Chen, Macromolecules **30**, 5104 (1997).
[15] N. Van Kampen, *Stochastic Processes in Physics and Chemistery* (Elsevier Science, Amsterdam, 2011).
[16] Y. Aharonov, L. Davidovich, and N. Zagury, Phys. Rev. A **48**, 1687 (1993).
[17] D. Meyer, J. Stat. Phys. **85**, 551 (1996).
[18] E. Farhi and S. Gutmann, Phys. Rev. A **58**, 915 (1998).
[19] F. W. Strauch, Phys. Rev. A **74**, 030301(R) (2006).
[20] G. H. Weiss, *Aspects and Applications of the Random Walk* (North-Holland, Amsterdam, 1994).
[21] O. Mülken and A. Blumen, Phys. Rep. **502**, 37 (2011).
[22] O. Mülken, V. Bierbaum, and A. Blumen, J. Chem. Phys. **124**, 124905 (2006).
[23] A. Anishchenko, A. Blumen, and O. Mülken, Quantum Inf. Process. **11**, 1273 (2012).
[24] O. Mülken, J. Stat. Phys. **162**, 644 (2016).
[25] G. Ritschel, J. Roden, W. T. Strunz, A. Aspuru-Guzik, and A. Eisfeld, J. Phys. Chem. Lett. **2**, 2912 (2011).
[26] G. Ritschel, J. Roden, W. T. Strunz, and A. Eisfeld, New J. Phys. **13**, 113034 (2011).
[27] A. M. Childs, Phys. Rev. Lett. **102**, 180501 (2009).
[28] I. Bloch, Nat. Phys. **1**, 23 (2005).
[29] B. C. Sanders, S. D. Bartlett, B. Tregenna, and P. L. Knight, Phys. Rev. A **67**, 042305 (2003).

[30] R. Côté, A. Russel, E. E. Eyler, and P. L. Gould, New J. Phys. **8**, 156 (2006).
[31] O. Mülken, A. Blumen, T. Amthor, C. Giese, M. Reetz-Lamour, and M. Weidemüller, Phys. Rev. Lett. **99**, 090601 (2007).
[32] W. Dür, R. Raussendorf, V. M. Kendon, and H.-J. Briegel, Phys. Rev. A **66**, 052319 (2002).
[33] M. Karski, L. Forster, J.-M. Choi, A. Steffen, W. Alt, D. Meschede, and A. Widera, Science **325**, 174 (2009).
[34] F. Zähringer, G. Kirchmair, R. Gerritsma, E. Solano, R. Blatt, and C. F. Roos, Phys. Rev. Lett. **104**, 100503 (2010).
[35] H. B. Perets, Y. Lahini, F. Pozzi, M. Sorel, R. Morandotti, and Y. Silberberg, Phys. Rev. Lett. **100**, 170506 (2008).
[36] A. Crespi, R. Osellame, R. Ramponi, V. Giovannetti, R. Fazio, L. Sansoni, F. De Nicola, F. Sciarrino, and P. Mataloni, Nat. Photon. **7**, 322 (2013).
[37] J. B. Spring *et al.*, Science **339**, 798 (2013).
[38] M. Tillmann, B. Dakić, R. Heilmann, S. Nolte, A. Szameit, and P. Walther, Nat. Photon. **7**, 540 (2013).
[39] M. A. Broome, A. Fedrizzi, S. Rahimi-Keshari, J. Dove, S. Aaronson, T. C. Ralph, and A. G. White, Science **339**, 794 (2013).
[40] A. Schreiber, A. Gárbis, P. P. Rohde, K. Laiho, M. Štefaňák, V. Potoček, C. Hamilton, I. Jex, and C. Silberhorn, Science **336**, 55 (2012).
[41] N. Kulvelis, M. Dolgushev, and O. Mülken, Phys. Rev. Lett. **115**, 120602 (2015).
[42] O. Mülken, M. Dolgushev, and M. Galiceanu, Phys. Rev. E **93**, 022304 (2016).
[43] A. A. Gurtovenko, D. A. Markelov, Yu. Ya. Gotlib, and A. Blumen, J. Chem. Phys. **119**, 7579 (2003).
[44] M. Galiceanu and A. Blumen, J. Chem. Phys. **127**, 134904 (2007).